

Superconducting Local Oscillators; Development and Optimization.

P.N. Dmitriev¹, L.V. Filippenko¹, K.V. Kalashnikov^{1,2}, M.E. Paramonov¹, K.I. Rudakov^{1,2}, and V.P. Koshelets^{1,*}

¹Kotel'nikov Institute of Radio Engineering and Electronics, Moscow, 125009, Russia

²Moscow Institute for Physics and Technology (State University), Dolgoprudny, Russia

*Contact: valery@hitech.cplire.ru, phone +7-495-6293418

Abstract— Different types of the superconductor local oscillators were considered for integration with a SIS-mixer to build fully superconducting integrated receivers (SIR). The Josephson Flux Flow Oscillators (FFO) based on Nb-AlOx-Nb and Nb-AlN-NbN junctions have proven to be the most developed for such integration. The continuous frequency tuning of the FFO over the 250 - 750 GHz frequency range and the possibility of FFO phase stabilization have been achieved. The output power of the FFO is sufficient to pump integrated on the same chip SIS mixer in a wide frequency range; the FFO power can be electronically adjusted. The FFO free-running linewidth has been measured between 0.3 and 5 MHz; resulting in the spectral ratio of the phase-locked FFO from 99 to 70% over the whole frequency range. The possibility of reaching the phase noise of the order of -90 dBc at an offset from a carrier frequency of more than 100 kHz has been demonstrated experimentally. To improve further FFO parameters and to extend its frequency range a number of new FFO designs were developed and investigated. The goal is to simplify the FFO operation at lower frequencies (through Fiske steps suppression at frequencies below Josephson self-coupling boundary) as well as to extend the FFO operation frequency beyond 1 THz. In this report an overview on development of superconducting integrated THz local oscillators is presented.

INTRODUCTION

Josephson junctions have been considered as natural terahertz oscillators for more than half a century, ever since Josephson discovered the effects named after him [1], [2]. Since that time, many quite different types of Josephson oscillators have been proposed and studied [3] – [13], but only a few of them were developed at level suitable for real applications. Let us consider one of the most attractive applications - the direct integration of a Josephson Local Oscillator (JLO) with the most sensitive heterodyne SIS mixer. There are a number of important requirements of the JLO's properties to make it suitable for application in the phase-locked Superconducting Integrated Receiver (SIR). The continuous frequency tuning of the JLO over a wide frequency range (usually more than 100 GHz) and a possibility of the JLO's phase stabilization at any frequency in the operation range are required for most applications. The output power of the JLO should be sufficient to pump the matched SIS mixer within a wide frequency range and it can be electronically

adjusted. Obviously, the JLO should emit enough power to pump an SIS mixer (of about 1 μ W), taking into account a specially designed mismatch of about 5–7 dB between the JLO and the SIS mixer, which should be introduced to avoid leakage of the input signal to the LO path. It is a challenge to realize the ultimate performance of the separate superconducting elements after their integration into a single-chip device. Another very important issue is the linewidth of the JLO. Even for wideband room-temperature PLL systems, the effective regulation bandwidth is limited by the length of the cables in the loop (about 10 MHz for a typical loop length of two meters). This means that the free-running JLO linewidth has to be well below 10 MHz to ensure stable JLO phase locking with a reasonably good spectral ratio (SR) — the ratio between the carrier and the total power emitted by the JLO.

NB-BASED FLUX-FLOW OSCILLATORS

The Josephson Flux Flow Oscillators (FFO) [14] – [19] based on Nb-AlOx-Nb and Nb-AlN-NbN junctions have proven [20] – [25] to be the most developed superconducting local oscillator for integration with an SIS mixer in a single-chip submm-wave Superconducting Integrated Receiver [26] – [29]. The FFO is a long Josephson tunnel junction of the overlapped geometry in which an applied DC magnetic field and a DC bias current, I_B , drive a unidirectional flow of fluxons, each containing one magnetic flux quantum, $\Phi_0 = h/2e \approx 2 \cdot 10^{-15}$ Wb. Symbol h represents Planck's constant and e is the elementary charge. An integrated control line with the current I_{CL} is used to generate the DC magnetic field that is applied to the FFO. According to the Josephson relation, the junction oscillates with a frequency $f = (I/\Phi_0) \cdot V$ (about 483.6 GHz/mV) if it is biased at voltage V . The fluxons repel each other and form a chain that moves along the junction. The velocity and density of the fluxon chain, and thus the power and frequency of the submm-wave signal emitted from the exit end of the junction due to the collision with the boundary, may be adjusted independently by the appropriate settings of I_B and I_{CL} . The FFO differs from the other members of the Josephson oscillator family by the need for these two control currents, which in turn provides the possibility of an independent frequency and power tuning.

We experimentally investigated a large number of the FFO designs. The length, L , and the width, W , of the FFO used in our study were 300–400 μm and 4–28 μm , respectively. The value of the critical current density, J_C , was in the range of 4–8 kA/cm^2 , giving a Josephson penetration depth of $\lambda_J \sim 6$ –4 μm . The corresponding value of the specific resistance was $R_n * L * W$ is ~ 50 –25 $\text{Ohm} * \mu\text{m}^2$. For the numerical calculations we used a typical value of the London penetration depth, $\lambda_L \approx 90$ nm for all-Nb junctions, and a junction-specific capacitance $C_s \approx 0.08$ $\text{pF}/\mu\text{m}^2$. The active area of the FFO (i.e., the AlO_x or the AlN tunnel barrier) is usually formed as a long window in the relatively thick (200–250 nm) SiO_2 insulation layer, sandwiched between the two superconducting films (the base and wiring electrodes). The so-called “idle” region consists of the thick SiO_2 layer adjacent to the junction (on both sides of the tunnel region) between the overlapping electrodes. It forms a transmission line parallel to the FFO. The width of the idle region ($W_1 = 2$ –14 μm) is comparable to the junction width. The idle region must be taken into account when designing an FFO with the desired properties. In our design, it is practical to use the flat-bottomed electrode of the FFO as a control line in which the current I_{CL} produces the magnetic field, which is mainly applied perpendicular to the long side of the junction.

Previously, the Nb- AlO_x -Nb or Nb- AlN -Nb trilayers were successfully used for the FFO’s fabrication. Traditional all-Nb circuits are constantly being optimized but there seems to be a limit for linewidth optimizations at certain boundary frequencies due to the Josephson self-coupling (JSC) effect [21], as well as a high frequency limit, imposed by the Nb gap frequency (~ 700 GHz). This is the reason to develop novel types of junctions based on materials other than Nb. We reported on the development of the high-quality Nb- AlN -NbN junction-production technology [30]. The implementation of an AlN tunnel barrier in combination with an NbN top superconducting electrode provides a significant improvement in the quality of the SIS junction. The gap voltage of the junction $V_g = 3.7$ mV. From this value, and the gap voltage of the Nb film $\Delta_{\text{Nb}}/e = 1.4$ mV, we have estimated the gap voltage of our NbN film as $\Delta_{\text{NbN}}/e = 2.3$ mV [25]. The use of Nb for the top “wiring” layer is preferable due to smaller losses of Nb when compared to NbN below 720 GHz. Furthermore, the matching structures developed for the all-Nb SIRs can be used directly for the fabrication of receivers with Nb- AlN -NbN junctions. The general behavior of the new devices is similar to that of the all-Nb ones; even the control currents, necessary to provide magnetic bias for the FFO, were nearly the same for the FFOs of similar designs.

A family of the Nb- AlN -NbN FFO IVCs, measured at different magnetic fields produced by the integrated control line, is presented in Fig. 1 ($L = 300$ μm , $W = 14$ μm , $W_1 = 10$ μm). A single SIS junction with an inductive tuning circuit was employed as a harmonic mixer (HM) for the linewidth measurements. The tuning and matching circuits were designed to provide “uniform” coupling in the frequency range of 400–700 GHz. Measured values of the HM current induced by the FFO oscillations (HM pumping) are shown in Fig. 1 by the color scale. The HM pumping for each FFO bias point was measured at a constant HM bias voltage of 3 mV

(pumping is normalized on the current jump at the gap voltage, $I_g = 140$ μA). From Fig. 1 one can see that an FFO can provide a large enough power over the wide frequency range, which is limited at higher frequencies only by the Nb superconducting gap in transmission line electrodes (base and wiring layers) and below 400 GHz by the design of the matching circuits.

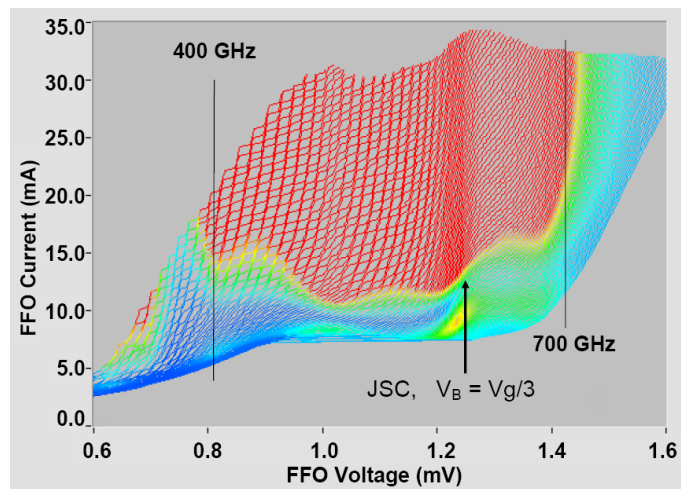


Fig. 1. IVCs of the Nb- AlN -NbN FFO, measured at different magnetic fields produced by the integrated control line. The color scale shows the level of the DC current’s rise at the HM induced by the FFO. The red area marks the region of the FFO’s parameters where the HM current induced by the FFO exceeds 25% of the I_g . This level is well above the optimal value for an SIS-mixer operation.

The feature at approximately 600 GHz where the curves get denser is a JSC (Josephson Self-Coupling) boundary voltage. It was initially observed for all-Nb FFOs [21]. The JSC effect is the absorption of the FFO-emitted radiation by the quasi-particles in the cavity of the long junction. It considerably modifies the FFO’s properties at the voltages $V \approx V_{JSC} = 1/3 * V_g$ (V_{JSC} corresponds to 620 GHz for the Nb- AlN -NbN FFO). Just above this voltage, the differential resistance increases considerably; that results in an FFO-linewidth broadening just above this point. This, in turn, makes it difficult or impossible to phase-lock the FFO in that region. For an Nb- AlO_x -Nb FFO, the transition corresponding to $V_{JSC} = V_g/3$ occurs around 450 GHz. Therefore, by using the Nb- AlN -NbN FFOs we can cover the frequency gap from 450 to 550 GHz that is imposed by the gap value of all-Nb junctions. The feature in Fig. 1 around 1 mV is very likely due to a singularity in the difference between the superconducting gaps $\Delta_{\text{NbN}} - \Delta_{\text{Nb}}$.

Continuous frequency tuning at frequencies below 600 GHz for the Nb- AlN -NbN FFOs of moderate length is possible, although the damping is not sufficient to completely suppress the Fiske resonant structure at frequencies below $V_g/3$. For short junctions with a small α (wave attenuation factor), the distance between the steps in this resonant regime can be as large, so that it is only possible to tune the FFO within a certain set of frequencies. For a 300–400 μm long Nb- AlN -NbN junction, this is not the case — the quality factor of the resonator formed by a long Nb- AlN -NbN Josephson junction is not so high at frequencies > 350 GHz. Therefore, the resonance steps are slanting and the distance between them is

not so large (see Fig. 1). This allows us to set any voltage (and any frequency) below V_{JSC} , but for each voltage, only a certain set of currents should be used. Therefore, in this case, we have the regions of forbidden bias-current values, which are specific for each voltage below V_{JSC} , instead of the forbidden voltage regions for the Fiske regime in Nb-AlOx-Nb FFO [25]. Special algorithms have been developed for automatic working-point selection in flight.

The typical current-voltage characteristics (IVCs) of an Nb-AlN-NbN SIS junction of an area approximately $1 \mu\text{m}^2$ is given in Fig. 2, which represents both the unpumped IVC (the solid line) and the IVC when pumped by an Nb-AlN-NbN FFO at different frequencies (dotted lines). One can see that the FFO provides more than enough power for the mixer pumping. In this experiment, we used the test circuits with low-loss matching circuits tuned between 400 and 700 GHz. Even with the specially introduced 5 dB FFO/SIS mismatch (required for the SIR operation), the FFO delivered enough power for the SIS mixer's operation in the TELIS frequency range of 400–700 GHz. An important issue for the SIR's operation is a possibility to tune the FFO's power, while keeping the FFO frequency constant. This is demonstrated in Fig. 3, where the IVCs of an SIS mixer pumped at the FFO frequency of 500 GHz are shown, while they were being pumped at different FFO bias currents (different powers). Our measurements demonstrated [24], [28] that the FFO power can be adjusted in the range of 0–15 dB while keeping the same frequency, by proper adjustment of the FFO control line current.

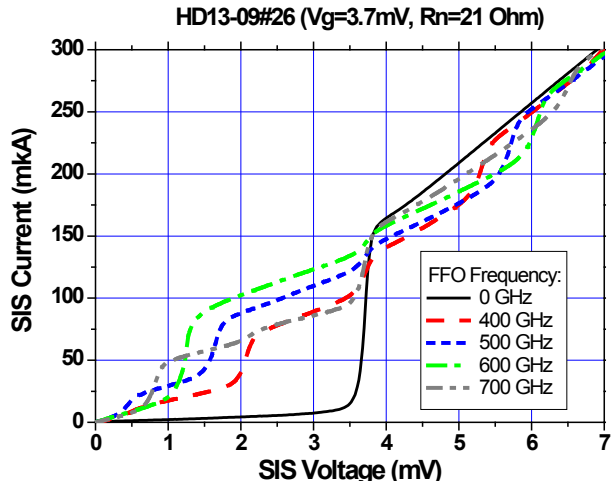


Fig. 2. The IVCs of the SIS mixer: unpumped = solid curve; pumped at different frequencies = dashed and dotted lines (color online).

LINEWIDTH OF THE FFO AND ITS PHASE-LOCKING

The FFO linewidth (LW) has been measured in a wide frequency range from 300 GHz up to 750 GHz by using a specially developed experimental technique [20] – [24]. A specially designed integrated circuit incorporates the FFO junction, the SIS harmonic mixer and the microwave matching circuits. Both junctions are fabricated from the same Nb/AlN/NbN or Nb/AlOx/NbN trilayer. A block diagram of the set-up for the linewidth measurements is described in [22].

The FFO signal is fed to the harmonic mixer (a SIS mixer operated in Josephson or quasiparticle mode) together with a 17–20 GHz reference signal from a stable synthesizer. The required power level depends on the parameters of the HM; it is about of $1 \mu\text{W}$ for a typical junction area of $1 \mu\text{m}^2$. The intermediate frequency (IF) mixer product ($f_{IF} = \pm (f_{FFO} - n \cdot f_{SYN})$) at ~ 400 MHz is first boosted by a cooled HEMT amplifier ($T_n 5$ K, gain = 30 dB) and then by a high-gain room-temperature amplifier.

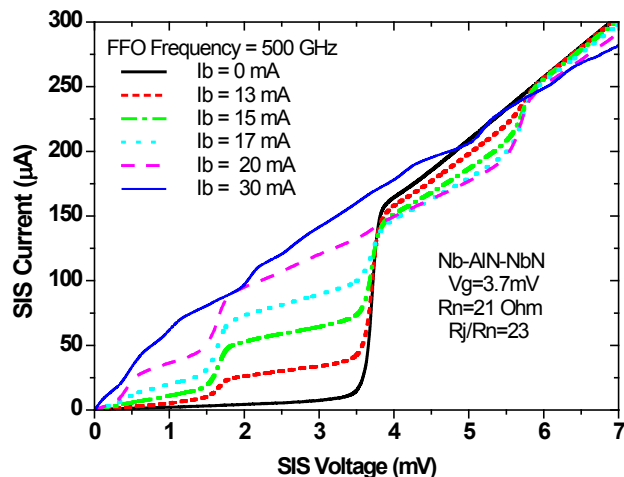


Fig. 3. The IVCs of the SIS mixer: unpumped = black solid curve; pumped at different FFO bias currents (different powers) = lines with symbols; FFO frequency = 500 GHz (color online).

In order to accurately measure the FFO line shape, the IF signal must be time-averaged by the spectrum analyzer. To remove low-frequency drift and interference from the bias supplies, temperature drift, etc., we used a narrow band (< 10 kHz) Frequency Discriminator (FD) system with a relatively low loop gain for the frequency locking of the FFO. With the FD narrow-band feedback system that stabilizes the mean frequency of the FFO (but which does not affect FFO's line shape), we can accurately measure the free-running FFO linewidth, which is determined by the much faster internal ("natural") fluctuations (see Fig. 4). The measured data are symmetrized relative to the center's frequency; these data are shown by diamonds. The profile of the FFO line recorded when biased at the steep Fiske step (FS), where the differential resistance is extremely small, can be different from the one measured on the smooth Flux Flow step. Theoretically [58], the shape is Lorentzian for wide-band fluctuations, while for narrow-band interference, at frequencies smaller than the autonomous FFO linewidth δf_{AUT} , the profile will be Gaussian; the theoretical curves are also shown in Fig. 4 for comparison. The theoretical lines providing the best fit near the peak are shown by the solid line and the dashed line for the Lorentzian and Gaussian profiles, respectively. The coincidence between the calculated curve and the symmetrized experimental data is excellent, and actually better than 5% in the emitted power, if a minor amplifier's nonlinearity of about 0.4 dB is taken into account.

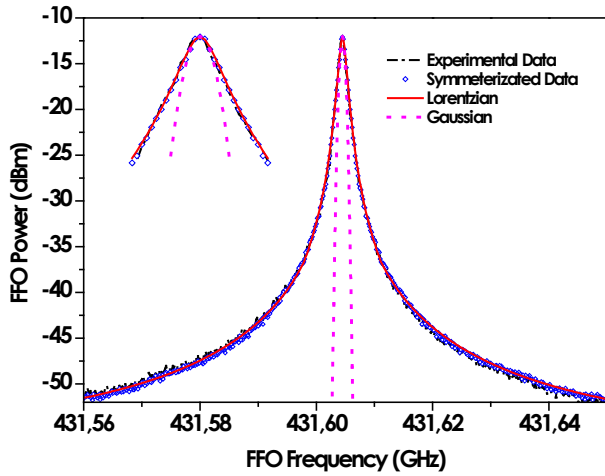


Fig. 4. The FFO spectrum measured when biased on the Fiske step ($V_{FFO} = 893 \mu\text{V}$, $R_d = 0.0033 \Omega$, $R_d^{Cl} = 0.00422 \Omega$, $\mathcal{J}_{AUT} = 1.2 \text{ MHz}$) is represented by the dash-dotted line. The symmetrized experimental data are shown by diamonds. The fitted theoretical Lorentzian and Gaussian profiles are shown by solid and dotted lines, respectively. The inset shows a close-up view of the central peak with the frequency axis multiplied five times [80].

The resulting IF signal is also supplied to the Phase-Locking Loop (PLL) system. The phase-difference signal of the PLL is fed to the FFO control-line current [15, 16, 75, 78–81]. Wideband operation of the PLL (10–15 MHz full width) is obtained by minimizing the cable loop’s length. A part of the IF signal is delivered to the spectrum analyzer via a power splitter (see Fig. 5, 6). All instruments are synchronized to the harmonics of a common 10 MHz reference oscillator. Dependencies of the free-running FFO linewidth and the Spectral Ratio (SR) for the phase-locked FFO on frequency for two different FFO technologies (Nb-Ox-Nb and Nb-AlN-NbN) are presented in Fig. 7. One can see that $\text{SR} > 70\%$ can be realized for Nb-AlN-NbN FFO in the range of 250–750 GHz.

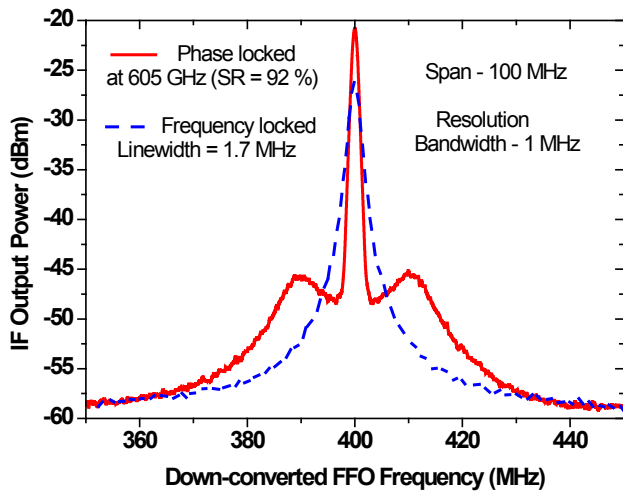


Fig. 5. Spectra of the Nb-AlN-NbN FFO operating at 605 GHz (blue dashed line = frequency locked by FD; red solid line = phase-locked). Linewidth = 1.7 MHz; Spectral Ratio = 92 % (color online).

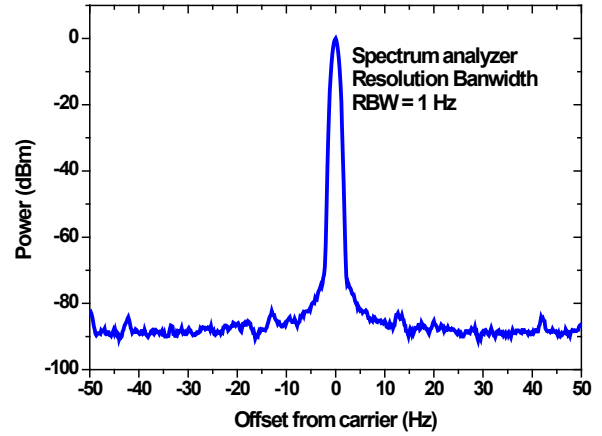


Fig. 6. Spectra of the phase-locked Nb-AlN-NbN FFO operating at 605 GHz. Span = 100 Hz, RBW = 1 Hz, signal-to-noise ratio = 87 dB as measured in a bandwidth of 1 Hz.

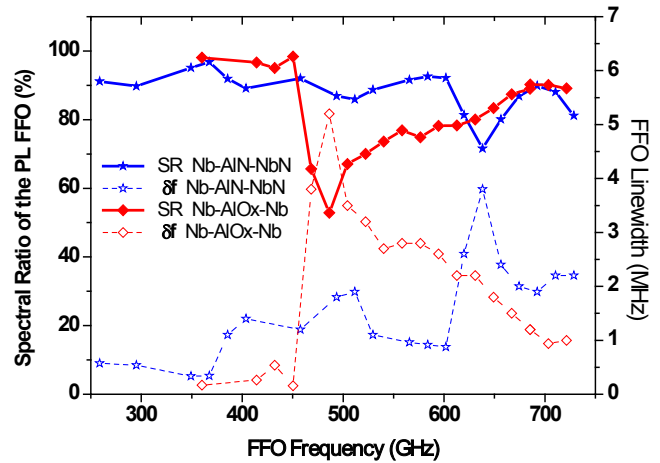


Fig. 7. Dependencies of the free-running FFO linewidth and the Spectral Ratio for the phase-locked FFO on frequency. Data are presented for two different FFO technologies: Nb-Ox-Nb (represented by diamonds) and Nb-AlN-NbN (asterisks).

CRYOGENIC PHASE DETECTOR

The local oscillator for the superconducting integrated receiver based on Flux flow oscillator has a tuning range of 250–750 GHz; in this range a free-run linewidth at half-height (-3 dB in power) may vary from hundreds kHz to several dozen of MHz (in some specific cases). When a conventional room-temperature (RT) PLL is used for the FFO phase locking, the FFO signal firstly down-converted at the harmonic mixer (HM) from hundreds of GHz to 400 MHz, and then the low frequency signal is amplified and sent from the cryostat to the semiconductor RT PLL. The phase of intermediate frequency signal is compared with the reference at the RT PLL, and the error signal is sent back to the cryostat, where it adjusts the FFO frequency. Long connecting cables are used to reduce the heat flow into the cryostat; however, it leads to a delay of the feedback signal of $\sim 10 \text{ ns}$. The electronic block of the PLL adds another 7 ns, resulting in a limitation of about 15 MHz for the synchronization band of the RT PLL for FFO.

For efficient locking of wide Lorentzian lines emitted by FFO a PLL system with a very wide regulation bandwidth is required (due to slow decrease of the noise level with offset

from the carrier). To overcome the limitations of the traditional RT PLL, we have developed the cryogenic high-harmonic phase detector (CHPD) [33], [34]. Implementation of the SIS junction both for down-conversion of oscillator frequency and generation of feedback signal to control the FFO frequency allows us to place all PLL elements in close vicinity to the oscillator. In turn, this provides significant reduction of loop time delay (less than 4 ns) and extremely large regulation bandwidth (up to 70 MHz). Since cryogenic PLL system consists of only superconductive and low-consumption elements, it could be integrated on the single chip with locked oscillator. As it is shown in Fig. 8, the CHPD PLL system could efficiently synchronize highly broad emission lines [29], [34].

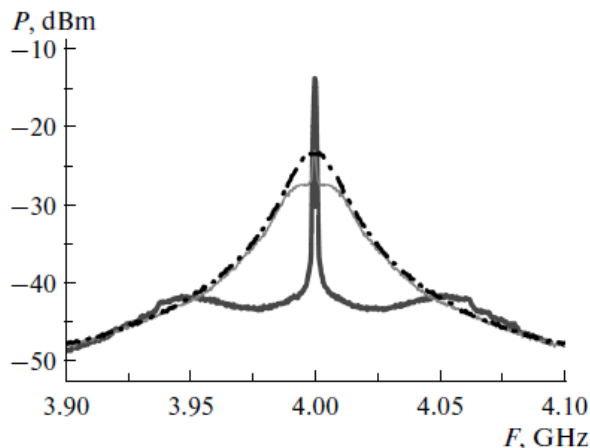


Fig. 8. Experimentally measured FFO emission spectra downconverted from 634 GHz. The dashed and dotted line represents the autonomous FFO oscillation spectrum (line width, 16.8 MHz); the thin line represents the FFO spectrum synchronized using a room-temperature PLL (spectrum ratio 6%). The bold line shows the FFO spectrum synchronized by CHPD (spectrum ratio 84%).

SUPPRESSION OF THE FISKE STEPS

As it was already mentioned, continuous tuning of the FFO frequency below $V_g/3$ is limited due to presence of the Fiske steps (see Fig. 1). To overcome this limitation and considerably suppress the Fiske resonances we have developed new FFO design with additional resistive elements (Fig. 9). It makes possible to increase damping and completely suppress the reflected electromagnetic waves and the Fiske resonant structure at frequencies just below $V_g/3$, see Fig. 10 and 11.

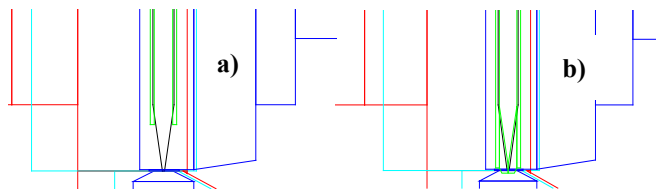


Fig. 9. Two layouts of the FFO with additional resistive elements (shown by green color) for suppression of the Fiske resonant structure at frequencies below $V_g/3$.

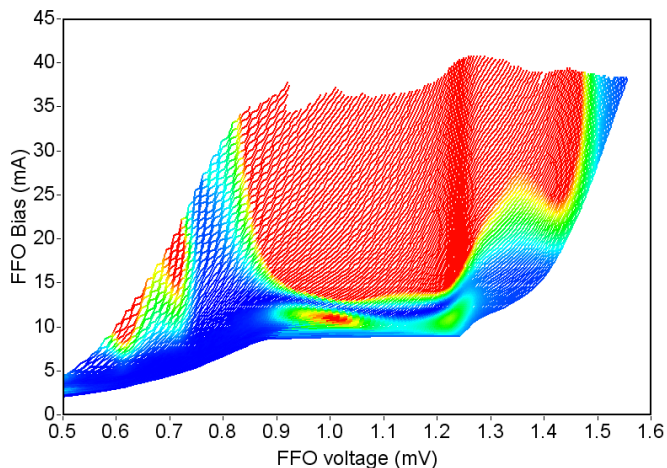


Fig. 10. IVCs of the Nb-AlN-NbN FFO with additional resistive elements for suppression of the Fiske resonant structure (design shown in Fig. 9 a); see Fig. 1 for comparison and detailed information/)

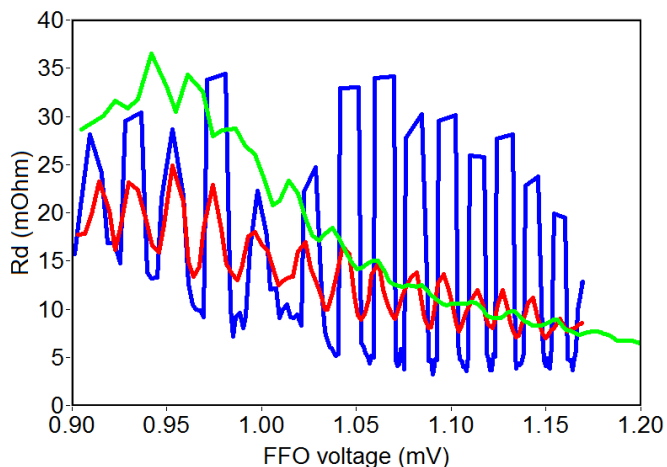


Fig. 11. The differential resistance of the FFO IVCs measured at FFO current of about 25 mA. Data for FFO without suppression (see Fig. 1) – blue curve; data for designs a) and b) are shown by red and green curves correspondingly.

CONCLUSIONS

The Flux Flow Oscillators (FFO) based on Nb-AlO_x-Nb and Nb-AlN-NbN junctions provide unique combination of parameters unreachable for any competing technique:

- 250 – 750 GHz tuning range (in practice might be limited by the SIS matching circuitry);
- FFO frequency and power can be electronically adjusted; furthermore FFO can be phase-locked at any frequency providing spectral ratio > 70 % with phase noise of the order of -90 dBc;
- FFO was integrated with an SIS mixer in a single-chip sub-THz Superconducting Integrated Receiver (SIR) for the atmospheric-research instrument Terahertz and submillimeter Limb Sounder (TELIS).

ACKNOWLEDGMENT

This work was supported by the Ministry of Education and Science of the Russian Federation (No. 14.607.21.0100; ID RFMEFI60714X0100).

REFERENCES

- [1] B.D. Josephson(1962). Possible new effects in superconductive tunnelling.*Phys. Lett.*1, pp. 251- 253.
- [2] B. D. Josephson, (1964). Coupled Superconductors, *Rev. Mod. Phys.* 36, pp. 216-220.
- [3] K. K. Likharev, Dynamics of Josephson Junctions and Circuits; Gordon and Breach, London, 1986.
- [4] C. Varmazis, R. D. Sandell, A. K. Jain, and J. E. Lukens, "Generation of coherent tunable Josephson radiation at microwave frequencies with narrowed linewidth", *Appl. Phys. Lett.* 33, 357 (1978).
- [5] A. K. Jain, K. K. Likharev, J. E. Lukens, and J. E. Sauvageau (1984). Mutual phase-locking in Josephson junction arrays. *Phys. Rep.* **109**, 309-426.
- [6] B. Dueholm, O. A. Levring, J. Mygind, N. F. Pedersen, O. H. Soerensen, and M. Cirillo (1981). Multisoliton Excitations in Long Josephson Junctions.*Phys. Rev. Lett.***46**, 1299.
- [7] Joergensen E., Koshelets V.P., Monaco R., Mygind J., Samuelsen M.R., Salerno M., "Thermal Fluctuations in Resonant Motion of Fluxon on a Josephson Transmission Line: Theory and Experiment", *Phys. Rev. Lett.*,**49**, pp. 1093-1096, (1982).
- [8] M. Cirillo and F. Lloyd (1987).Phase lock of a long Josephson junction to an external microwave source. *J. Appl. Phys.***61**, 2581.
- [9] P. A. A. Booi and S. P. Benz (1994).Emission linewidth measurements of two-dimensional array Josephson oscillators, *Appl. Phys. Lett.***64**, 2163.
- [10] Barbara, P., Cawthorne, A. B., Shitov, S. V. and Lobb, C. J. (1999). Stimulated Emission and Amplification in Josephson Junction Arrays,*Phys. Rev. Lett.***82**, pp. 1963-1965.
- [11] Morvan Salez and Faouzi Boussaha, Fluxon modes and phase-locking at 600 GHz in superconducting tunnel junction nonuniform arrays, *Journal of Applied Physics* 107, 013908 (2010).
- [12] Song, F., Müller, F., Scheller, T., Semenov, A. D., He, M., Fang, L., Hübers, H.-W. and Klushin, A. M. (2011). Compact tunable subterahertz oscillators based on Josephson junctions, *Appl. Phys. Lett.***98**, 142506.
- [13] M A Galin, A M Klushin, V VKurin, S V Seliverstov, M I Finkel, G N Goltsman, F Müller, T Scheller and A D Semenov, "Towards local oscillators based on arrays of niobium Josephson junctions", *Supercond. Sci. Technol.* **28** (2015) 055002 (7pp)
- [14] Nagatsuma, T., Enpuku, K., Irie, F. and Yoshida, K. (1983). Flux-flow type Josephson oscillator for millimeter and submillimeter wave region. *J. Appl. Phys.* **54**, 3302.
- [15] Nagatsuma, T., Enpuku K., Sueoka K., Yoshida, K. and Irie F., Flux-flow type Josephson oscillator for millimeter and submillimeter wave region. II. Modeling, *J. Appl. Phys.* **56**, 3284 (1984).
- [16] Nagatsuma, T., Enpuku, K., Yoshida, K. and Irie F. (1985). Flux-flow type Josephson oscillator for millimeter and submillimeter wave region. III. Oscillation stability, *J. Appl. Phys.* **58**, 441.
- [17] J. Qin, K. Enpuku and K. Yoshida, Flux-flow type Josephson oscillator for millimeter and submillimeter wave region. IV. Thin-film coupling, *J. Appl. Phys.* **63**, 1130 (1988).
- [18] Y. M. Zhang and P. H. Wu, J. (1990). Numerical calculation of the height of velocity-matching step of flux-flow type Josephson oscillator, *Appl. Phys.* **68**, 4703-4709.
- [19] Y. M. Zhang, Winkler, T. Claeson (1993). Detection of mm and submm wave radiation from soliton and flux-flow modes in a long Josephson junction," *IEEE Trans. Appl. Superconductivity*, **3**, pp. 2520 – 2523
- [20] Koshelets V P, Shitov S V, Shchukin A V, Filippenko L V, and Mygind J, "Linewidth of Submillimeter Wave Flux-Flow Oscillators". *Appl. Phys. Lett.***69** 699-701 (1996)
- [21] Koshelets V P, Shitov S V, Shchukin A V, Filippenko L V, Mygind J, and Ustinov A V. "Self-Pumping Effects and Radiation Linewidth of Josephson Flux Flow Oscillators". *Phys Rev B***56** 5572-5577 (1997)
- [22] V.P. Koshelets, S.V. Shitov, A.V. Shchukin, L.V. Filippenko, P.N. Dmitriev, V.L. Vaks, J. Mygind, A.M. Baryshev, W. Luinge, H. Golstein, "Flux Flow Oscillators for Sub-mm Wave Integrated Receivers", *IEEE Trans. on Appl. Supercond.* 9, 4133–4136 (1999).
- [23] Koshelets V P and Mygind J, "Flux Flow Oscillators For Superconducting Integrated Submm Wave Receivers", *Studies of High Temperature Superconductors*, edited by A.V. Narlikar, NOVA Science Publishers, New York, **39** 213-244 (2001)
- [24] Koshelets V. P., Dmitriev P. N., Ermakov A. B., Sobolev A. S., Torgashin M. Yu., Kurin V. V., Pankratov A. L., Mygind J. (2005). Optimization of the Phase-Locked Flux-Flow Oscillator for the Submm Integrated Receiver, "*IEEE Trans. on Appl. Supercond.*", **15**, pp.964-967
- [25] M.Yu. Torgashin, V.P. Koshelets, P.N. Dmitriev, A.B. Ermakov, L.V. Filippenko, and P.A. Yagoubov, "Superconducting Integrated Receivers based on Nb-AlN-NbN circuits" "*IEEE Trans. on Appl. Supercond.*", vol. 17, pp.379- 382, 2007.
- [26] V. P. Koshelets, S. V. Shitov, L. V. Filippenko, A. M. Baryshev, H. Golstein, T. de Graauw, W. Luinge, H. Schaeffer, H. van de Stadt "First Implementation of a Superconducting Integrated Receiver at 450 GHz"; *Appl. Phys. Lett.*, 68, 1273 (1996).
- [27] V.P. Koshelets, S.V. Shitov, "Integrated Superconducting Receivers" *Superconductor Science and Technology*, vol 13, pp. R53-R69, (2000).
- [28] V.P. Koshelets, M. Birk, D. Boersma, J. Dercksen, P.N. Dmitriev, A.B. Ermakov, L.V. Filippenko, H. Golstein, R. Hoogeveen, L. de Jong, A.V. Khudchenko, N.V. Kinev, O.S. Kiselev, P.V. Kudryashov, B. van Kuik, A. de Lange, G. de Lange, I.L. Lapitsky, S.I. Pripolzin, J. van Rantwijk, A. Selig, A.S. Sobolev, M.Yu. Torgashin, V.L. Vaks, E.de Vries, G. Wagner, P.A. Yagoubov, "Integrated Submm Wave Receiver: Development and Applications", - Chapter in the book "Nanoscience Frontiers - Fundamentals of Superconducting Electronics", Springer Serie: Nanoscience and Technology 35372, pp. 263-296, Editor: Anatolie Sidorenko (August 2011).
- [29] V.P. Koshelets, P.N. Dmitriev, M.I. Faley, L.V. Filippenko, K.V. Kalashnikov, N.V. Kinev, O.S. Kiselev, A.A. Artanov, K.I. Rudakov, A. de Lange, G. de Lange, V.L. Vaks, M.Y. Li, H.B. Wang, "Superconducting Integrated Terahertz Spectrometers", *IEEE Transactions on Terahertz Science and Technology*, vol. 5, pp 687- 694, (July 2015).
- [30] P.N. Dmitriev, I.L. Lapitskaya, L.V. Filippenko, A.B. Ermakov, S.V. Shitov, G.V. Prokopenko, S.A. Kovtonyuk, and V.P. Koshelets. "High Quality Nb-based Integrated Circuits for High Frequency and Digital Applications", "*IEEE Trans. on Appl. Supercond.*", vol. 13, No 2, pp. 107-110, 2003.
- [31] Koshelets V P, Ermakov A B, Dmitriev P N, Sobolev A S, Baryshev A M, Wesselius P R, Mygind J, "Radiation linewidth of flux flow oscillators", *Superconductor Science and Technology* **14** 1040 – 1043 (2001)
- [32] V.P. Koshelets, S.V. Shitov, L.V. Filippenko, V.L. Vaks, J. Mygind, A.B. Baryshev, W. Luinge, N. Whyborn, "Phase Locking of 270-440 GHz Josephson Flux Flow Oscillator", *Rev. of Sci. Instr.*, v. 71, No 1, pp. 289-293, (2000).
- [33] A. V. Khudchenko, V. P. Koshelets, P. N. Dmitriev, A. B. Ermakov, P. A. Yagoubov and O.M. Pylypenko, "Cryogenic Phase Locking Loop System for Superconducting Integrated Receiver", *Supercond.Sci. and Technol.*,**22**,085012 (2009).
- [34] Kalashnikov, K.V., Khudchenko, A.V. and Koshelets, V.P. (2013). Harmonic Phase Detector for Phase Locking of Cryogenic Terahertz Oscillator, *Appl. Phys. Lett.* **103**, pp.102601-1-102601-4.